A NOVEL APPROACH TO ADDRESS THE BOTTLENECKS OF OPTICAL PAYLOADS ON NANOSATELLITES.

Thys Cronje[(1)], Eben Grobbelaar[(1)], Jacu Vos[(1)], Gregor Dreijer[(1)], Ana-Mia Louw[(1)], Chantel Botha[(1)], Johann du Toit[(1)]

(1) Simera Sense, Old Paardevlei Road, Somerset West, South Africa, +27(0)218526450, thys.cronje@simera.com

The trend towards significant constellations of smaller earth observation satellites is gaining fast momentum. Until recently, high-end earth observation satellites mainly were bespoke systems, and at best, a constellation was limited to a few satellites, while smaller earth observation satellites were primarily experimental. Today, nanosatellites are increasingly used for earth observation with a solid drive to tap into the commercial remote sensing market.

The drive to launch constellations of nanosatellites for commercial earth observation introduces new challenges to the manufacturing approach. It is driven by three significant factors: the demand for more detail (spatial, spectral, and radiometric), reduced form factors, and lower cost. These challenges are further elevated by the specific needs of the new space industry to rapidly iterate and scale production while providing value at the lower end of the market.

However, nanosatellites have limitations when addressing the traditional bottlenecks within the imaging chain. This paper introduces a novel approach to cost-effectively producing optical payloads by using lean procedures while maintaining quality and performance. This approach addresses design choices to (1) optimize resolution within a small form factor, (2) reduce the per-unit cost, (3) increase payload efficiency, (4) standardize on interfaces, and (5) go beyond pixels.

The solutions presented include end-to-end optical and environmental test results and inflight results from sub-5m and sub-2m GSD instruments for 3U/6U/16U nanosatellites. For all the solutions, the front aperture is stretched to the limits imposed by the spacecraft to maximize the diffraction limit. The engineering team utilized athermal design principles to compensate for the limited thermal control on the smaller spacecraft.

The two solutions, with inflight results, to be presented include:

- a 95mm aperture, 580mm focal length, 1.5U volume optical instrument available in RGB/Video, eight bands multispectral and 16 bands hyperspectral options with an optical MTF of >18%.
- a 190 mm aperture, 1067mm focal length, 12U volume optical instrument available in RGB/Video, and eight bands multispectral options with an optical MTF of >18%.

In addition, options to improve the inflight radiometric performance and data efficiency are discussed.

This approach to production at scale optical payloads for smaller satellites creates the opportunity to cost-effectively launch constellations of commercial earth observation satellites while maintaining performance across a wide range of environmental conditions.

1 INTRODUCTION

Earth Observation from space is a standard tool to assess and monitor changes on the earth's surface and the immediate environment [1]. Since Earth Observation data became available for civilian use in the early 1970s with the Landsat program, it created the backbone for land surface monitoring and characterization. The Multispectral Camera onboard Landsat 1, called the Multispectral Scanner System (MSS), paved the way for other satellites and the development of remote sensing applications [3][5]. The four spectral bands used on this satellite, green, red, and two Near-IR bands, became the international standard. These spectral bands also enabled the scientific community to develop multiple vegetation index algorithms to analyze and classify imagery. Today, Landsat 8, designed with eleven spectral bands, and Sentinel-2 with 13 bands, cover the visible, near-IR, Short Wave Infra-red, and thermal infrared bands. Most satellite optical payloads reflect this trend of using multispectral cameras. In 2021, 9% of the 1743 small satellites launched carried a remote sensing payload [9].

This rapid development of the earth observation domain and the demand for fresh data has increased the need for lean and agile space missions [3][4]. Over the last decade, nanosatellites have evolved from pure educational and scientific tools to providing commercially viable platforms for various payload options. Therefore, nanosatellites lead the way to a crossroad where space and IT meet. Historically, the traditional providers of EO satellites, services, and data ignored this shift by relying on old business models focusing on governmental and military needs. Today, we also see that other performance criteria are becoming more critical apart from the spatial resolution. This includes surface area captured per day, latency and reactivity, image freshness, video capabilities, hyperspectral capabilities, automatic calibration and processing, data delivery mechanisms, and capital and operational costs [3][5].

Given this shift in user needs and the market landscape (e.g., cost, revisit time, global coverage), nanosatellites are becoming attractive for Earth Observation. Table 1 captures the current trends driving the EO nanosatellite market and the challenges faced by this market.

Table 1: Trends and challenges in the EO nanosatellite market.

TRENDS	CHALLENGES
Bus commoditization	Not all satellite busses are equal
Rideshare traction	Long time-to-market for new space entrants
Faster revisit – mega-constellations	Long latency for ground-in-the-loop responsiveness
Application-specific focus	Unrealistic resolution expectations
Increase in compute in space	Increase sensor data volume eclipse data bandwidth

A new value chain is evolving for EO nanosatellites due to the changes within the EO nanosatellite landscape. These changes impact satellite and sensor manufacturers, integration, test providers, launch service providers, communication systems, calibration and downstream processing, archiving and distributed data, and general satellite operations.

Commercially minded entrepreneurs would like to believe that Moore's Law can also be applied to optical payloads and Earth Observation - that the pixel density on a focal plane would

double approximately every two years and, therefore, the spatial resolution. But unfortunately, an optical payload's diffraction limit is still the most critical performance parameter.

Therefore, this paper covers the main parameters that create bottlenecks within the performance of an optical payload onboard a nanosatellite and how they impact the instrument accuracy. Specific design choices are addressed, and results from the xScape100 and xScape200 products for 3U to 16U Cubesats are presented.

2 INSTRUMENT ACCURACY LIMITATIONS

The nanosatellites' low-cost advantage comes with some constraints and inefficiencies. These constraints are mainly driven by the satellite's limited form factor, commercial component selection, and reduced development time, resulting in accuracy limitations [10].

For all practical considerations, an Earth Observation instrument is a measurement device translating emitted or reflected energy from the earth's surface and surroundings into an image where each pixel acts as a measurement point. These measurements are used for spatial mapping purposes, the radiometric quantization of reflected energy, the object's spectral content, and to determine temporal changes. From an end-user perspective, the question is, how accurate must the measurement be to address a specific challenge. These accuracies are summarized within the following four categories:

1. **Spatial Accuracy** (Resolution) – determines the smallest resolvable object or target in the field of view at a given orbital height, atmospheric conditions, and signal level.
2. **Radiometric Accuracy** (Sensitivity) – defines the smallest signal from an object or variation in signal in the presence of noise that can be detected.
3. **Spectral Accuracy** – The smallest spectral variations that can be detected within an object function of the number of spectral bands and their associated spectral resolution.
4. **Temporal Accuracy** – The shortest expected duration within which spatial, radiometric, or spectral changes can be quantified within a given object.

2.1 SPATIAL ACCURACY

Spatial accuracy determines the smallest distance that objects can be apart and still be distinguished from each other. This parameter is mainly dictated by the system application and is frequently expressed as Ground Sampling Distance (GSD). Over the last decade, the tendency was to push the GSD as small as possible within a given form factor satellite. Therefore, in nanosatellites, the goal is to transfer as much spatial detail as possible from the object on the earth's surface to the optical payload's imaging plane. It should be remembered that the GSD is only a geometric scaling of the pixel pitch (x_{det}) to the orbital height (H)/focal length (f_l) ratio [6][7]:

$$GSD\ (\mathrm{m}) = \frac{H}{f_l}\, x_{det} \qquad (1)$$

As the options to select specific orbital heights (H) or perform orbital manoeuvres with a nanosatellite are limited, the two parameters that need optimization are the pixel pitch (x_{det}) and the effective focal length (f_l). These two parameters are frequently scaled together to achieve a compact optical design. However, a smaller pixel pitch increases the system Nyquist

Sampling Frequency (f_{nyq}), adding complexity to the optical design. Where f_{nyq} is calculated as [6][7]:

$$f_{nyq} = \frac{1}{2\,x_{det}} \qquad (2)$$

with x_{det} expressed in millimeters, f_{nyq}, is given in cy/mm.

The optical Q factor also needs some consideration when selecting the pixel dimensions. The rule of thumb is that imaging systems for human observation typically are optimized for an optical Q-factor of between one and two ($1 < Q < 2$), whereas radiometric processing requirements are optimized for a Q-factor between 0.3 and one ($0.3 < Q < 1$). The optical Q-factor is defined as [8]:

$$Q_{factor} = \frac{\lambda f_{\#}}{x_{det}} \qquad (3)$$

with

$$f_{\#} = \frac{f_l}{D_{op}} \qquad (4)$$

Due to diffraction, we model an optical instrument as a low pass filter. In this case, the spatial cut-off frequency (f_{CO}) quantifies the limit beyond which the system would not be able to resolve any spatial detail. The spatial cut-off frequency is indirectly proportional to the optical wavelength (in millimeter) and F# of the system [6][7]:

$$f_{CO} = \frac{1}{\lambda f_{\#}}\ cycles/millimeter \qquad (5)$$

Ground resolved distance (GRD) relates to the diffraction-limited resolution of an optical system. The GRD determines the smallest distance that two objects can be apart for the system to be still able to distinguish between the two objects. This calculation brings the power of the optical system into the equation, something the geometric GSD calculator fails to do. The GRD is directly proportional to the orbital height and the spectral wavelength and indirectly proportional to the system's aperture diameter [8]:

$$GRD = 1.22\,\frac{\lambda}{D_{op}}\ Orbital\ Height \qquad (6)$$

The following figure provides a plot of GRD as a function of aperture diameter at spectral wavelengths of 550 nm and 850 nm and an orbital height of 500 km.

When considering all the elements that could influence the spatial resolution of an imaging instrument, the Modulation Transfer Function (MTF) is maybe the best parameter to describe the end-to-end imaging performance. The MTF models spatial resolution performance as a low pass filter, quantifying the amount of contrast transferred from the object to the image. The elements in the MTF model could include the atmospheric effects, the optical system limitation, the effect due to ADCS instabilities (jitter and smear), and the sensor's constraints. As we express MTF in the frequency domain, the system MTF is a multiplication of all the underlying subsystem's MTFs:

$$MTF_{System} = MTF_{Atmosphere} \times MTF_{Optics} \times MTF_{Jitter} \times MTF_{Smear} \times MTF_{Detector} \quad (7)$$

Due to the scanning motion nature of an Earth Observation satellite's optical payload, one-pixel smear in the along-track direction is expected. The result is a loss of about 35% in MTF in the along-track direction. In addition, low-frequency roll and yaw movements during the exposure time may influence the across-track MTF. Scanning or pixel misalignment when performing Time Delay Integration imaging degrade MTF further and needs to be added to eq. (7).

We model jitter as a Gaussian blur due to high-frequency vibrations within the satellite structure. Jitter has a significant impact on the MTF and must be preferably limited to less than 10% of a pixel during a typical integration time (rule-of-thumb).

2.2 RADIOMETRIC ACCURACY

Radiometric accuracy or sensitivity is determined by the maximum amount of uncertainty tolerated within the reflected and measured signal that would still allow unambiguous discrimination between measurements. For a nanosatellite optical payload, it is necessary to relate the reflected energy to electrons in a pixel, as this addresses most of the radiometric bottlenecks within the optical chain. The signal in electrons per pixel captured during the pixel integration time is [6][7]:

$$N_s = \frac{\Omega\, A_{pixel} T_{int} n_{tdi}}{hc} \int_0^{\infty} L_{source}(\lambda)\, \lambda\, QE(\lambda)\, \tau_{opt}(\lambda) d\lambda \quad (8)$$

Within eq. (8), $\Omega\, A_{pixel}$ provides the "throughput" of an optical imaging system, T_{int} is the pixel integration time, n_{tdi} are the number of time-delay and integration stages, λ is the wavelength, QE(λ) is the detector spectral quantum efficiency, $\tau_{opt}(\lambda)$ is the optical system spectral transmittance, including obscuration and filters, $L_{source}(\lambda)$ is the spectral radiance, h is Planck's constant, and *c* is the speed of light.

Ω is the solid angle subtended by the optical aperture as viewed from the detector plane and calculated as [6][7]:

$$\Omega = \frac{\pi}{4\,(f_{\#})^2} \quad (9)$$

And A_{pixel} is the area of a pixel [6][7]:

$$A = x_{det}^2 \quad (10)$$

The integration time, T_{int}, is the time it takes for a pixel to travel the distance of one GSD. Integration time is calculated as the GSD divided by the corresponding ground speed for a nadir-looking system. When applying forward motion compensation (FMC) utilizing slew rate control, T_{int} increase by the FMC factor applied.

The optical system's transmittance is a function of the spectral filter properties ($\tau_{filter}(\lambda)$), optical element transmittance ($\tau_{tr}(\lambda)$) and the linear obscuration ratio (ε_{obs}) [6][7].

$$\tau_{opt}(\lambda) = \tau_{tr}(\lambda)\, \tau_{filter}(\lambda)\, (1 - \varepsilon_{obs}{}^2) \quad (11)$$

The radiometric accuracy of the system is optimized by making N_S as large as possible. This optimization can be done by increasing the pixel size, integration time (with FMC), the number

of TDI stages or minimizing the $f_{\#}$. On the other hand, maximizing the overall optical transmittance or selecting a detector with higher quantum efficiency increases N_S.

Another way to increase SNR, especially if a traditional TDI detector is not available, is to use digital time delay integration. With this method, the same area on the earth is scanned multiple times by consecutive pixels. These pixels are then added to reduce the noise utilizing averaging.

2.3 SPECTRAL ACCURACY

Standard off-the-shelf cameras, like those in your mobile phone, are optimized to take pictures that represent, as close as possible, what the eye can see. These cameras use a color filter array, known as a Bayer filter mosaic, with a Red, Green, and Blue (RGB) filter distributed on a matrix of photosensors (pixels).

Commercial cameras use a demosaicing algorithm to interpolate the red, green, and blue values for each pixel to recreate the spectral content for each pixel. These pretty pictures are great to capture the moment but have limited value when going beyond detecting, identifying, and classifying objects. It should also be noted that the spectral bands of commercial RGB detectors do overlap, making spectral analysis quite complex.

Spectral content is one of the most important parameters when analyzing Earth Observation data, as it can provide information beyond what is visible. Multispectral and hyperspectral cameras can sample the spectral reflectance from an object at multiple wavelengths across a broad spectrum to identify the spectral "footprint" of the object. However, these spectral bands need to be well-defined for a specific application. Furthermore, overlapping of adjacent spectral bands needs to be prevented.

The spectral range covered by an optical imaging system is mainly driven by the spectral response of the underlying technology the detector utilizes. However, the optical design may become more complex if accuracy is required across a wide spectral range.

The number of spectral bands, and their spectral width and position within the spectrum, are a function of the application. The higher the variation in spectral content or the more diverse applications, the more spectral bands are required.

2.4 TEMPORAL ACCURACY

The most significant impact that Earth Observation nanosatellites can make is to increase the temporal accuracy to see and monitor change. In addition, the reduction in spacecraft and launch costs makes the continuous monitoring of the planet a reality. However, specific design choices on a payload, satellite, and mission level can impact the number of satellites required to cover the planet.

For example, by doubling the swath of an instrument, the number of satellites required for a specific revisit time can be reduced significantly.

3 OPTICAL PAYLOAD DESIGN APPROACH

Simera Sense primarily designed the xScape100 and xScape200 range of imagers to fit in standard 3U, 6U, and 16U nanosatellite bus structures. The goal of these optical payloads is to provide an off-the-shelf solution that can address the needs of the nanosatellite Earth Observation market in terms of cost and performance expectations.

3.1 OPTO-MECHANICAL DESIGN

The main challenge is to optimize the design for the available form factor within a nanosatellite structure to address all the bottlenecks, especially the aperture diameter and focal length. Figure 1 and Figure 2 show the approach followed to optimize the design.

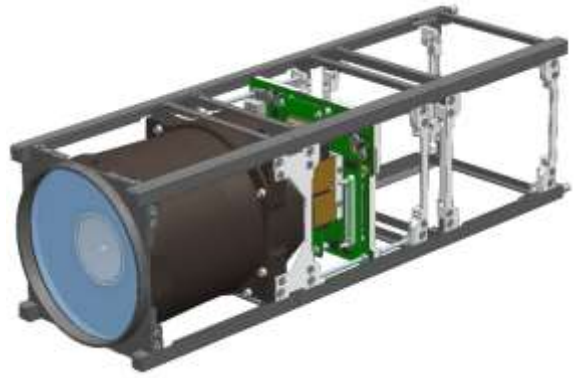

Figure 1: The xScape100 mechanical layout within a 3U Cubesat bus structure provided by **ISISpace**.

Figure 2: The xScape200 mechanical layout within a 16U Cubesat bus structure provided by **NanoAvionics**.

In both cases, a modified Cassegrain optical design is used to bring performance to the edge of the field over a wide spectral range (450 nm to 900 nm) at ultra-low distortion. As the primary performance driver for the Optical Front-End (OFE) is the effective aperture, this parameter is stretched to the limits in both cases. Due to the structure of nanosatellites, the following front aperture limits (including mechanical fixtures) are applied for the target structures:

- 3U/6U structure: ≤ 98 mm x 98 mm
- 16U structure: ≤ 216 mm x 216m

Furthermore, the available space within the system, in combination with the GSD requirements, drives the focal length optimization.

The size of commercial off-the-shelf detectors determined the image plane sizes of the respective payload solutions:

- 3U/6U structure: APS-C like detector (the CMV 12000 was selected)
- 16U structure: 35 mm full-frame detector (the GMAX3265 detector was selected)

The respective OFEs were designed to maintain performance across a relatively wide thermal range. A passively athermal design approach was followed with the optimal performance within the following targeted thermal environment:

- Operating temperature (soak): -10°C to +50°C
- Maximum Axial temperature gradient: 3°C
- Maximum transverse temperature gradient: 2°C

The environmental vibration targets are 14.1 g_{rms} and 10.0 g_{rms} (in all directions) for the medium- and high-resolution payloads.

3.2 IMAGER ELECTRONICS DESIGN

The detector is based on a CMOS imaging sensor with various filter options in the visible and near-infrared (VNIR) spectral range. A modular design approach is followed where all the payloads across the product range use identical control electronics.

The imager employs continuous line-scan imaging with digital time delay integration (dTDI) for multispectral and hyperspectral imaging solutions. In addition, the push frame and video-enabled versions of these imagers employ an RGB Bayer pattern detector.

4 XSCAPE100 AND XSCAPE200 PERFORMANCE SUMMARY

4.1 SPATIAL ACCURACY

As expressed in Section 2.1, spatial accuracy is mainly expressed as MTF, GRD, and GSD, where GSD is the most frequently used parameter. Table 2 provides a breakdown of all the parameters directly impacting the spatial accuracy.

However, two critical parameters that directly impact spatial accuracy are a function of the spacecraft's Attitude Determination and Control System (ADCS) and any micro-vibrations originating within the spacecraft. Therefore, it is recommended that the RMS jitter (high-frequency vibrations) during the integration time should be limited to 10% or less of a pixel's instantaneous field of view.

On the other hand, smear (low-frequency roll, pitch, yaw) must not be more than one pixel within the along-track direction. Smear in the across-track direction must be kept close to zero. However, as smear MTF follows a sinc(x)/x profile, the impact is not as severe as high-frequency jitter. As the integration time increases with FMC and the number of dTDI stages applied, the stability requirements on the ADCS also increase.

Table 2: A comparison of the parameters determining the spatial accuracy of the xScape100 and xScape200 product ranges.

xScape100	xScape200
Aperture Diameter: 95 mm	**Aperture Diameter**: 190 mm
Focal Length: 580 mm	**Focal Length**: 1067 mm
F#: 6.1	**F#**: 5.6
Obscuration Diameter: 47.2 mm	**Obscuration Diameter**: 84.4 mm
Distortion: < 0.165%	**Distortion**: <0.04%
Pixel Size: 5.5 µm	**Pixel Size**: 3.2 µm
Instantaneous Field of View: 0.54 mdeg	**Instantaneous Field of View:** 0.17 mdeg
Nyquist Frequency: 91 lp/mm	**Nyquist Frequency**: 156.3 lp/mm
OFE On-Axis MTF at 632.8 nm and 20 ˚C • ≥ 18.5% from 0 – 93 lp/mm	**OFE On-Axis MTF** at 632.8 nm and 20 ˚C • ≥ 17% from 0 – 157 lp/mm
Ground Resolved Distance (GRD): • 3.5 m @ 550 nm (Q-factor: 0.61) • 5.5 m @ 850 nm (Q-factor: 0.94)	**Ground Resolved Distance (GRD)**: • 1.77 m @ 550 nm (Q-factor: 0.94) • 2.73 m @ 850 nm (Q-factor: 1.45)

Ground Sampling Distance (GSD): 4.75 m @ 500 km	**Ground Sampling Distance (GSD)**: 1.5 m @ 500 km
System MTF at Nyquist (simplified): ($MTF_{System} = MTF_{Imager} \times MTF_{Jitter} \times MTF_{Smear}$)	System MTF at Nyquist (simplified): ($MTF_{System} = MTF_{Imager} \times MTF_{Jitter} \times MTF_{Smear}$)
Along-Track / **Across-Track** MTF_{Imager} 12.0% / 12.0% MTF_{Jitter} 95.2% / 95.2% MTF_{Smear} 63.7% **MTF_{System} 7.3% / 11.4%**	**Along-Track** / **Across-Track** MTF_{Imager} 11.0% / 11.0% MTF_{Jitter} 95.2% / 95.2% MTF_{Smear} 63.7% **MTF_{System} 6.7% / 10.5%**
Jitter Stability Requirements: Limited to 10% of a pixel MTF at Nyquist: 95.2% ADCS Req. (FMC = 1, # dTDI = 1): 80.9 mdeg/sec ADCS Req. (FMC = 2, # dTDI = 6): 40.4 mdeg/sec	**Jitter Stability Requirements**: Limited to 10% of a pixel MTF at Nyquist: 95.2% ADCS Req. (FMC = 1, # dTDI = 1): 80.9 mdeg/sec ADCS Req. (FMC = 4, # dTDI = 10): 20.2 mdeg/sec
Smear Stability Requirements: One Pixel Smear MTF: 63.7% ADCS Req. (FMC = 1, # dTDI = 1): 809 mdeg/sec ADCS Req. (FMC = 2, # dTDI = 6): 67 mdeg/sec	**Smear Stability Requirements:** One Pixel Smear MTF: 63.7% ADCS Req. (FMC = 1, # dTDI = 1): 809 mdeg/sec ADCS Req. (FMC = 4, # dTDI = 10): 20 mdeg/sec

4.2 RADIOMETRIC ACCURACY

As shown in Section 2.2, the main driver for radiometric accuracy is the system's F-number. Hence, for a given GSD, the effective aperture diameter, taking the obscuration and transmittance into account, is the determining factor when optimizing radiometric accuracy.

The radiometric accuracy of nanosatellite EO systems is mainly limited by quantum noise or photon noise due to the low levels of noise contributed by the detector. Therefore, to reduce the contributing effect of shot noise, the number of photons captured must be maximized or the noise minimized.

This improvement in radiometric parameters can be made by increasing the integration time, lowering the relative ground speed with FMC, and averaging the effect of shot noise with digital time delay integration.

Table 3: A comparison of the parameters determining the radiometric accuracy of the xScape100 and xScape200 product ranges.

xScape100	xScape200
Aperture Diameter: 95 mm	**Aperture Diameter**: 190 mm
Obscuration Diameter: 47.2 mm	**Obscuration Diameter**: 84.4 mm
F#: 6.1	**F#**: 5.6
Optical Transmittance (without obscuration): >85%	**Optical Transmittance (without obscuration)**: >83%
Field of View: 2.96°	**Field of View**: 2.01°
Pixel Size: 5.5 µm	**Pixel Size**: 3.2 µm
Pixel Solid Angle: $9x10^{-12}$ sr	**Pixel Solid Angle:** $9x10^{-12}$ sr
Full Well Capacity: 13 500 e^-	**Full Well Capacity**: 10 900 e^-

Quantum Efficiency: 50% peak	**Quantum Efficiency:** 65% peak
Dynamic Range: 60 dB	**Dynamic Range**: >66dB at 12-bit
Dark Current: 70 e^-/pixel/sec @ 25°C	**Dark Current:** 5.3 e^-/pixel/sec @ 40°C
Temporal Noise: 13 e^-	**Temporal Noise:** 1.9e^- @ x6 Gain
Pixel Integration time (FMC=1): 672 µs	**Pixel Integration time (FMC=1)**:
Digital Quantization: 12 bits	**Digital Quantization: 12 bits**:
Number of digital TDI (dTDI) stages: 6 recommended	**Number of digital TDI (dTDI) stages**: 10 recommended
Forward Motion Compensation: 2 recommended	**Forward Motion Compensation**: 4 recommended

Table 4 and Table 5 provide an overview of the expected signal-to-noise parameters for the MultiScape100 and MultiScape200 instruments. In addition, the specific FMC and dTDI parameters used and the at aperture radiance must be noted, as this has a significant impact on the radiometric accuracy.

Table 4: The radiometric performance of the MultiScape200 with at aperture radiance of 100 W/m^2/sr/um and FMC = 4 and dTDI = 10.

	B1	B2	B3	B4	B5	B6	B7
Central Wavelength [nm]	490	560	665	705	740	783	842
Electrons per pixel	1 604	839	507	242	215.55	222	865
Signal to Noise Ratio	122	86	64	41	37	38	87

Table 5: The radiometric performance of the MultiScape100 with at aperture radiance of 100 W/m2/sr/um and FMC = 2 and dTDI = 6.

	B1	B2	B3	B4	B5	B6	B7
Central Wavelength [nm]	490	560	665	705	740	783	842
Electrons per pixel	3 937	2 190	1 866	966	945	1 082	4 659
Signal to Noise Ratio	150	110	101	70	69	75	164

Figure 3 includes the negative effect of the obscuration on the total spectral transmission. However, it should be noted that the obscuration size is a crucial factor in determining the field size and, therefore, the swath of the system.

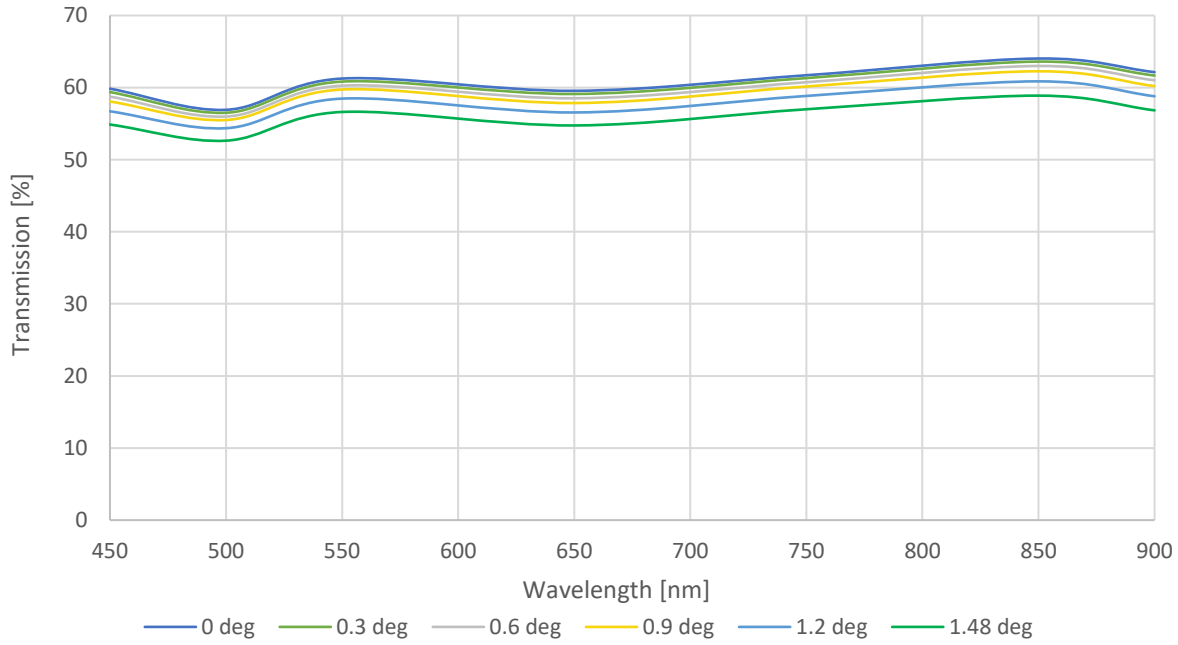

Figure 3: Transmission (Obscuration Included) across the spectral range at different angles for the xScape100 VNIR OFE.

4.3 SPECTRAL PERFORMANCE

4.3.1 RGB VISIBLE SPECTRAL PERFORMANCE

The TriScape100 and TriScape200 optical payloads utilize detectors with commercial off-the-shelf RGB Bayer pattern spectral bands, as shown in Figure 4. It should be noted that the spectral responses displayed in Figure 4 include the detector's quantum efficiency. Furthermore, as these spectral bands are optimized to create visually appealing images, there is an overlap between the bands, making spectral analysis complex.

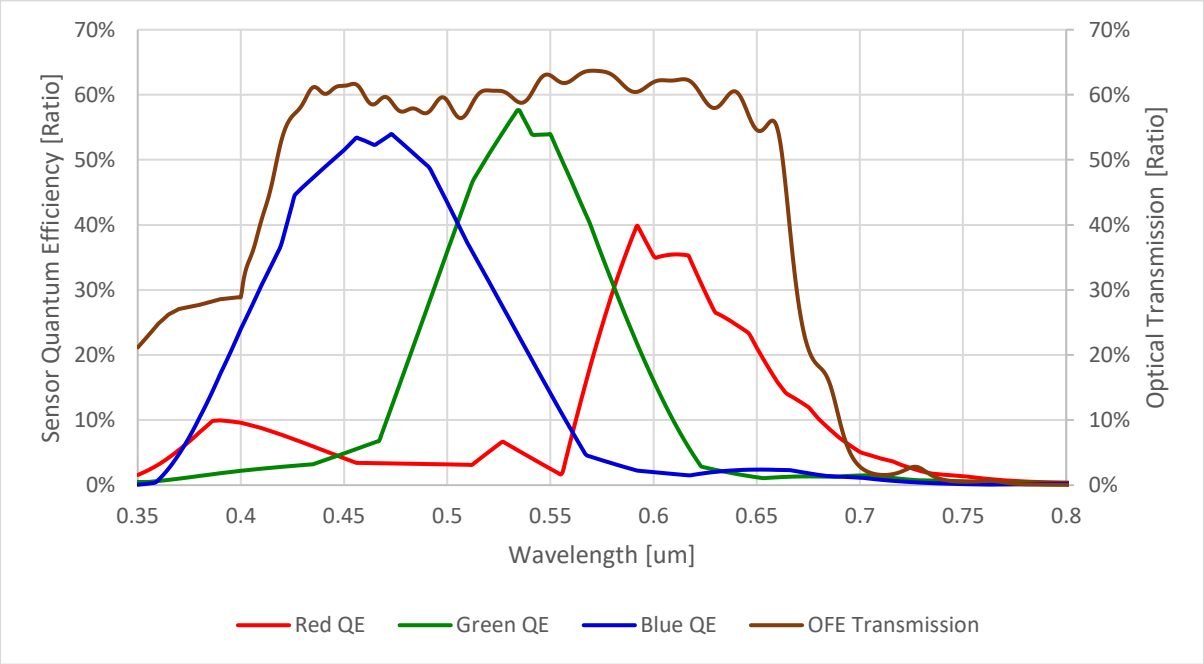

Figure 4: The RGB Bayer pattern and optical transmission spectral response.

4.3.2 MULTISPECTRAL PERFORMANCE

An eight-band butcher block configuration on a glass substrate integrated within a CMOS imaging sensor is used for the multispectral optical payload solutions. The windowing mode of the sensor allows capturing the eight spectral bands in a push broom operational mode.

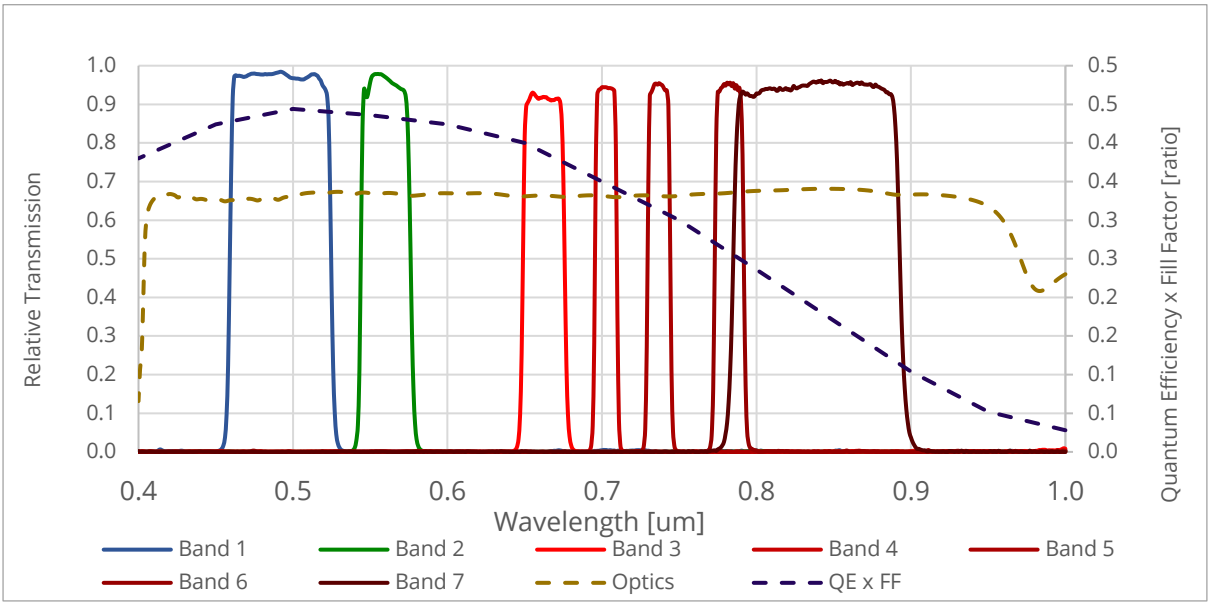

Figure 5: The filter spectral transmission bands, the detector Quantum Efficiency, and the OFE transmission.

4.4 TEMPORAL ACCURACY

Data freshness, and therefore the frequency at which geospatial data of a specific area on earth could be delivered, is the main driver for many nanosatellite applications. From a mission operational perspective, there are two ways to address data freshness:

- Capture every point on the earth at a regular interval, e.g., daily, or
- Capture any point on the earth at a regular interval.

However, the main driver to increase temporal accuracy from a payload perspective is swath, where swath is a function of the field size corresponding to the detector active area size. One thing that should be kept in mind, with an increase in temporal resolution, data handling also becomes more complex.

Table 6: A comparison of the parameters determining the temporal accuracy of the xScape100 and xScape200 product ranges.

xScape100	xScape200
Ground Sampling Distance: 4.75 m	Ground Sampling Distance: 1.5 m
Field Size / diameter: 30 mm	Field Size / diameter: 38 mm / 45 mm
Along-track pixel count: 4096 pixels	Along-track pixel count: 9 344 pixels
Swath: 19.42 km	Swath: 14.01 km

Off-nadir viewing: Sideway viewing is a spacecraft limitation to capture any point.	Off-nadir viewing: Sideway viewing is a spacecraft limitation to capture any point.

In both cases, the respective instruments acquire a large number of pixels when covering the earth's land surface. For a full land surface coverage with MultiScape100 at 4.75 m GSD about 6.6 terapixels are captured, and 66.2 terapixels for the MultiScape200 at 1.50 m GSD. The above numbers must be multiplied by eight when using all the spectral bands. Therefore, the system's ability to handle large volumes of data is an essential factor to consider when evaluating temporal accuracy.

5 RESULTS

Both the xScape100 and xScape200 product ranges are fully qualified for space. A MultiScape100 was launched on a 6U Cubesat, with the resulting unprocessed images shown below. These images are used to validate the multispectral instrument's spatial, radiometric, and spectral accuracy.

Ultimately, the spatial, radiometric, and spectral accuracy is a function of the pre-and post-launch instrument characterization and calibration activities.

SPATIAL ACCURACY

By comparing the RAW multispectral images with Sentinel-2 reference data, jitter within the attitude data of the spacecraft can be characterized. Furthermore, by implementing orthorectification stages, adequate ground control points can improve the attitude and ephemeris data. Therefore, it must be noted that spatial accuracy is a function of the instrument's spatial resolution and a combination of satellite stability and sufficient and accurate attitude information.

SPECTRAL ACCURACY

It should be noted that spectral accuracy is not only a function of the system's spectral range, number of spectral bands, and shape of the bands but also alignment between the bands. By design, the spectral bands are separated across the focal plane and therefore do not image the same area at the same instance. Therefore, any high-frequency jitter or low-frequency roll, pitch, and yaw movements (smear) between the bands while imaging impact spectral accuracy. Disparity maps between the spectral bands must be generated to correct these spectral inaccuracies, and the resulting translation maps must be applied to the pixel data.

RADIOMETRIC ACCURACY

Pre- and post-launch detector bias and gain characterization must be performed to create an accurate geometric model. In addition, flat-field correction and de-striping need to be applied during the radiometric calibration steps, both pre-and post-launch, to increase the radiometric accuracy of the instrument.

Figure 6: An urban area captured with Band 0 (uncorrected) of the MultiScape100.

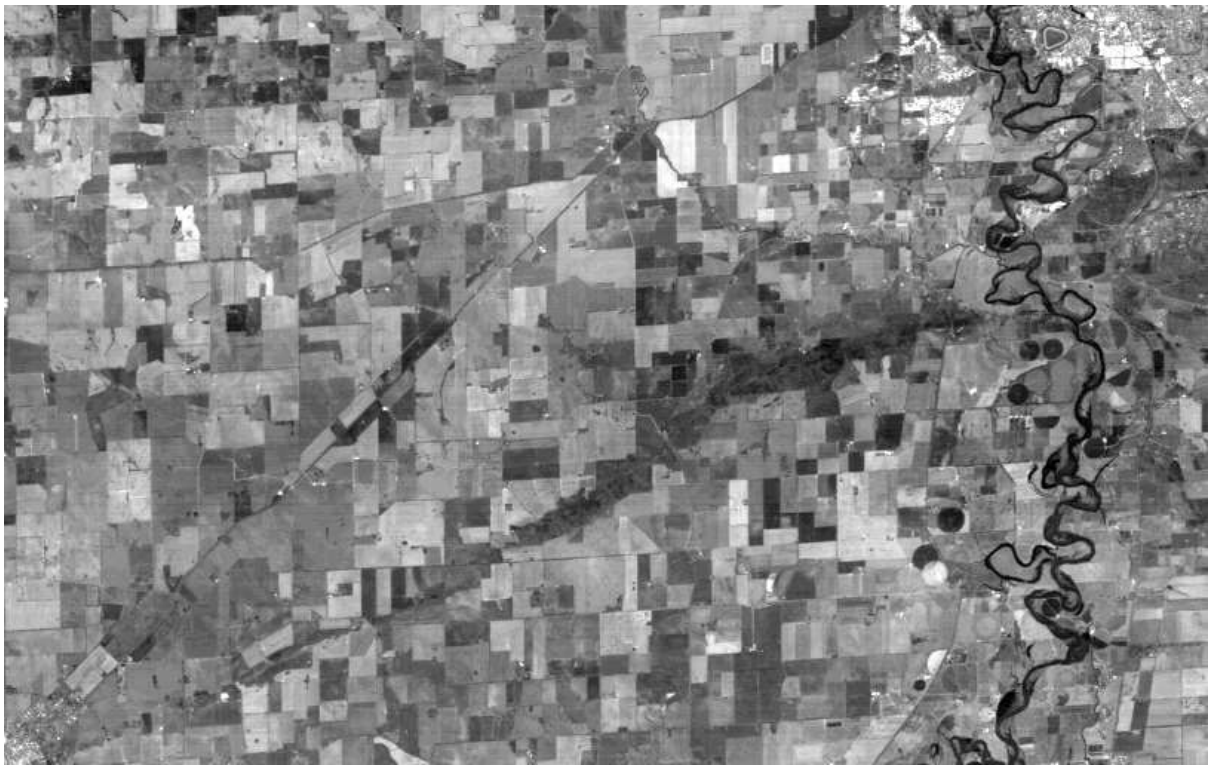

Figure 7: A rural area captured with Band 0 (uncorrected) of the MultiScape100.

6 ACKNOWLEDGEMENTS

It is with great pleasure to thank our nanosatellite bus partners, ISISpace and NanoAvionics, for flying our respective instruments on their missions and providing valuable feedback. We would also like to thank Pink Matter Solutions for processing the images and determining the spatial, spectral, and radiometric accuracies.

7 REFERENCES

[1] SANDAU, R. *Status and Trends of Small Satellite Missions for Earth Observation* Acta Astronautica, v. 66, n. 1-2, p. 1-12, 2010. https://doi.org/10.1016/j.actaastro.2009.06.008

[2] SANDAU, R.; BRIE, K.; ERRICO, M. D. Small, *Satellites for Global Coverage: Potential and Limits*, ISPRS Journal of Photogrammetry and Remote Sensing, v. 65, n. 6, p. 492-503, 2010. https://doi.org/10.1016/j.isprsjprs.2010.09.003

[3] Denis, G., et al. *Towards disruptions in Earth observation? New Earth Observation systems and markets evolution: Possible scenarios and impacts*, Acta Astronautica. 137. 10.1016/j.actaastro.2017.04.034.

[4] Praks J., et al. *AALTO-1 earth observation cubesat mission — Educational outcomes*, 2015 IEEE International Geoscience and Remote Sensing Symposium (IGARSS), 2015, pp. 1340-1343, doi: 10.1109/IGARSS.2015.7326023.

[5] van Genderen, J., et al. (2019). *Digital Earth Challenges and Future Trends*, 10.1007/978-981-32-9915-3_26.

[6] Terrence S. Lomheim, Erich D. Hernandez-Baquero, *Translation of spectral radiance levels, band choices, and signal-to-noise requirements to focal plane specifications and design constraints*, Proc. SPIE 4486, Infrared Spaceborne Remote Sensing IX, (8 February 2002); https://doi.org/10.1117/12.455111

[7] Bradly J., et al. *Methodology for rapid infrared multispectral electro-optical imaging system performance analysis and synthesis*, Proc. SPIE 2743, Infrared Imaging Systems: Design, Analysis, Modeling, and Testing VII, (10 June 1996); https://doi.org/10.1117/12.241949

[8] Robert F., *Image quality and [lambda]FN/p for remote sensing systems*, Opt. Eng. 38(7) (1 July 1999) https://doi.org/10.1117/1.602169

[9] Smallsats by numbers, Bryce Tech, https://brycetech.com/reports

[10] Nagel G., et al. Nanosatellites applied to optical Earth observation: a review, Ambient. Água 15 (3), 2020, https://doi.org/10.4136/ambi-agua.2513